GAEP0117-23-113
Tracking Star-Forming Cores as Mass Reservoirs in Clustered and Isolated Regions Using Numerical
Passive Tracer Particles
by Nozaki, S. et al. ApJ

GAEP0117-23-75
The Fragmentation of Molecular Clouds in Starburst Environments
by Matt T. Cusack et al. MNRAS in press

GAEP0117-23-50
ALMA chemical survey of disk-outflow sources in Taurus (ALMA-DOT) VII: the layered molecular outflow from HL
Tau and its relationship with the ringed disk
by F. Bacciotti et al. A & Ap in press

GAEP0117-23-16
Vertical structure and kinematics of the LMC disc from SDSS/Gaia by O. Jimenez-Arranz et al. AAp in press

GAEP0117-23-120
JOYS: The [D/H] abundance derived from protostellar outflows across the Galactic disk measured with JWST by L.
Francis et al, A&Ap in press

GAEP0117-23-07
Detectability of Emission from Exoplanet Outflows Calculated by pyTPCI, a New 1D Radiation-Hydrodynamic
Code by Riley Rosener et al. ApJ in press

Tracking Star-Forming Cores as Mass Reservoirs in Clustered and Isolated Regions Using Numerical Passive Tracer Particles by Nozaki, S. et al. ApJ 九大

Understanding the physical properties of star-forming cores as mass reservoirs for protostars, and the impact of turbulence, is crucial in star formation studies. We implemented passive tracer particles in clump-scale numerical simulations with turbulence strengths of $\mathcal{M}_{rms} = 2, 10$. Unlike core identification methods used in observational studies, we identified 260 star-forming cores using a new method based on tracer particles falling onto protostars. Our findings reveal that star-forming cores do not necessarily coincide with high-density regions when nearby stars are present, as gas selectively accretes onto protostars, leading to clumpy, fragmented structures. We calculated convex hull cores from star-forming cores and defined their filling factors. Regardless of turbulence strength, convex hull cores with lower filling factors tend to contain more protostars and have larger masses and sizes, indicating that cores in clustered regions are more massive and larger than those in isolated regions. Thus, the filling factor serves as a key indicator for distinguishing between isolated and clustered star-forming regions and may provide insights into the star formation processes within clustered regions. We also found that most convex hull cores are gravitationally bound. However, in the $\mathcal{M}_{rms} = 10$ model, there are more low-mass, unbound convex hull cores compared to the $\mathcal{M}_{rms} = 2$ model. In the $\mathcal{M}_{rms} = 10$ model, 16% of the convex hull cores are unbound, which may be explained by the inertial-inflow model. These findings highlight the influence of turbulence strength on the mass and gravitational stability of cores.

観測的には高密度の一連のガス塊で定義される、
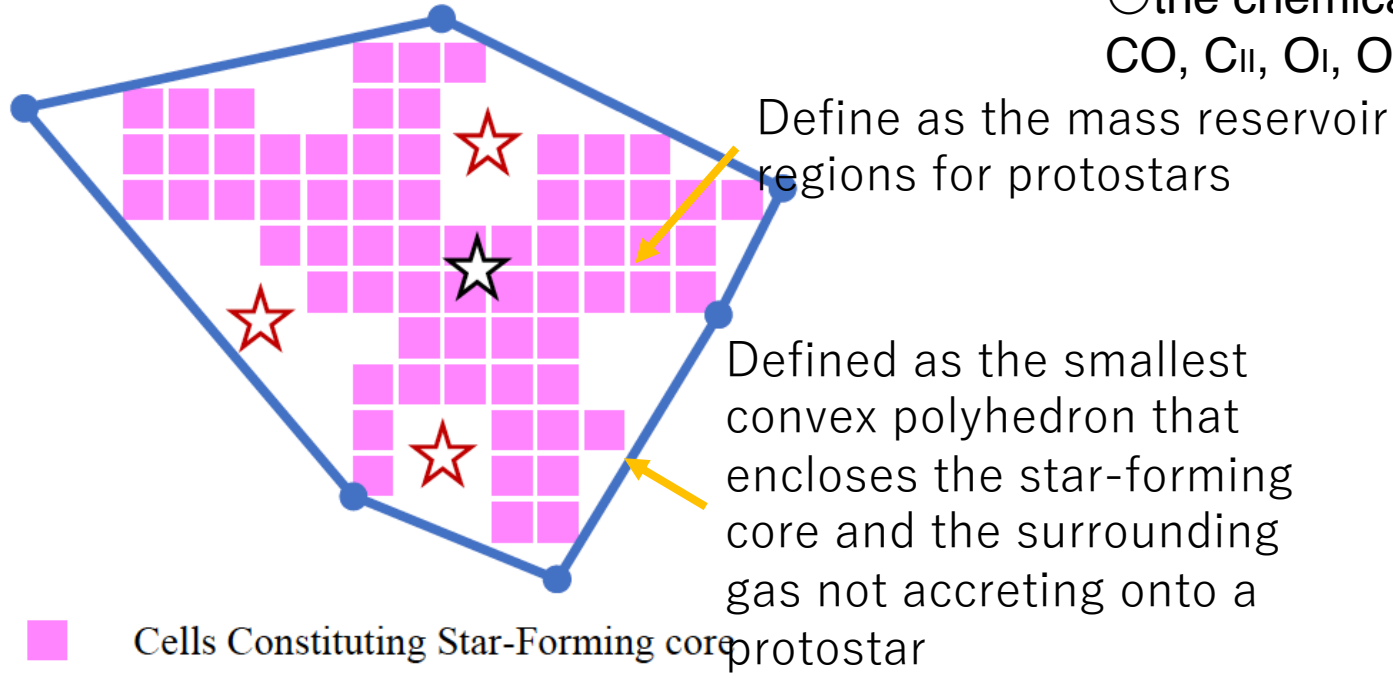原始星へ降着するガスはどこから来るかという観点で、Star Forming Coreを定義して
その性質を調べる

方法
AMR流体計算で乱流ガスの進化を追跡。$n_{sink}=9 \times 10^6 cm^{-3}$以上にシンク粒子
L=4pc、6段AMRで、Δx=195au、n0=1365cm-3、Mrms=2,10モデル、スペクトル$P(k) \propto k^{-4}$
最初の原始星形成時から1Myr追跡

独自
初期に一様に置かれた流跡粒子を追跡

○heating: from chemical reactions,
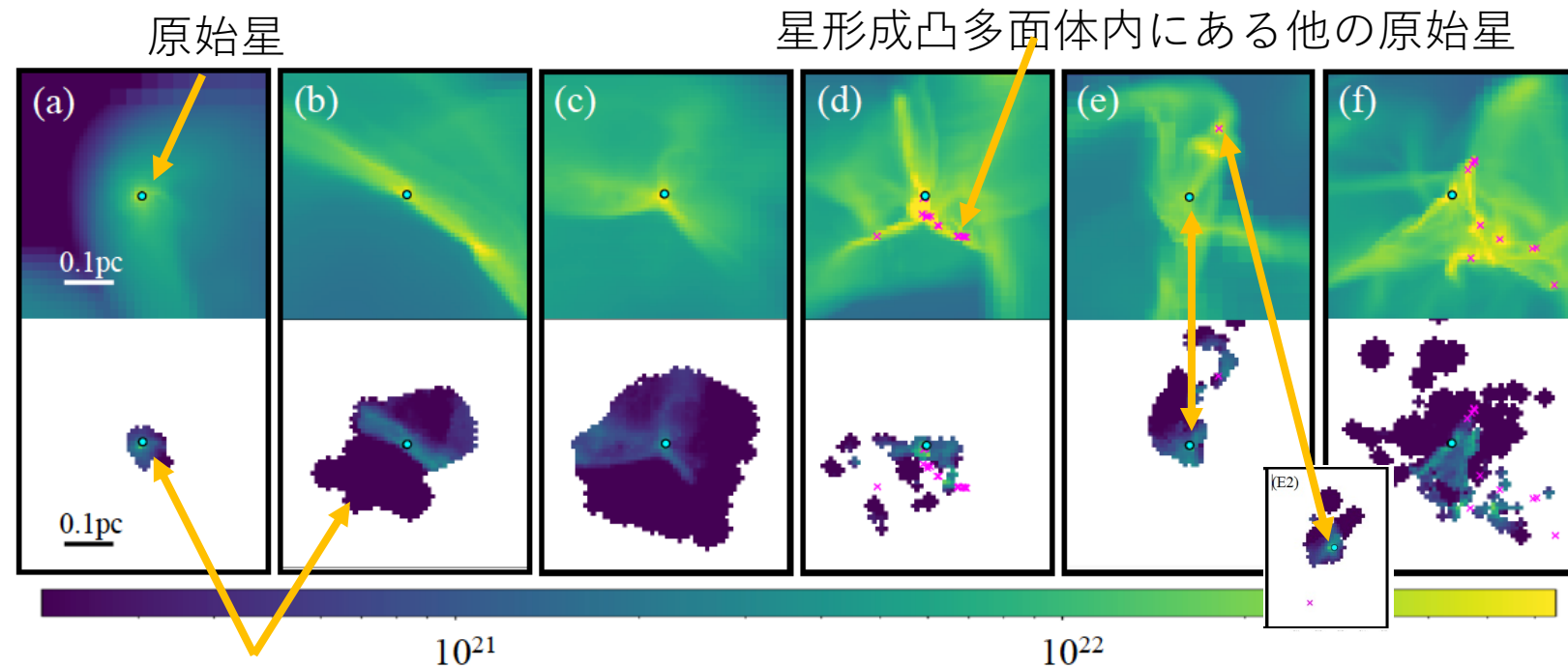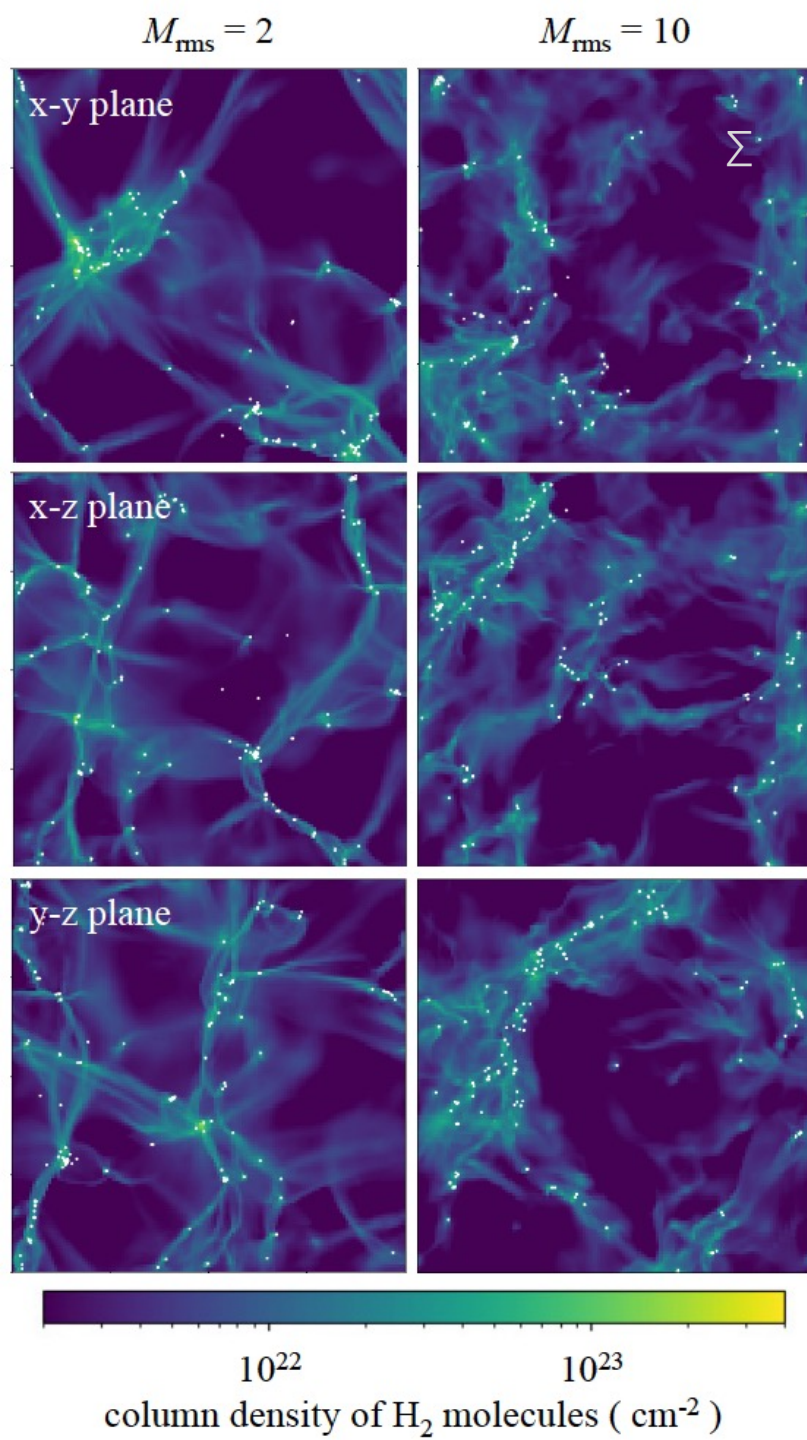○cooling: from line emissions and energy transfer between gas and dust.
○the chemical network of 11 species: H, H_2, H^-, H^+, H^+_2, e, CO, C_{II}, O_I, O_{II}, and O_{III}

Define as the mass reservoir regions for protostars

Defined as the smallest convex polyhedron that encloses the star-forming core and the surrounding gas not accreting onto a protostar

★星形成コア
(A)0.3Myr以内にシンク粒子☆に降着する流跡粒子をidする。
(B)各粒子から以下の距離以下のセルの集合

$$r_{i,\text{particle}} = \left(\frac{3M_{\text{particle}}}{4\pi\rho_{\text{cell}}} \right)^{\frac{1}{3}}$$

■ Cells Constituting Star-Forming core

●— Convex Hull Cores' Edges　凸多面体

☆ Protostar as Final Destination for Gas within Star-Forming Core

☆ Other Protostars in the Region

$M_{rms} = 2$

$M_{rms} = 10$

x-y plane

Σ

0.1pc

x-z plane

y-z plane

10^{22} 10^{23}

column density of H$_2$ molecules (cm^{-2})

原始星

星形成凸多面体内にある他の原始星

(a) (b) (c) (d) (e) (f)

0.1pc

0.1pc

(E2)

10^{21} 10^{22}

Column density of H$_2$ molecules N_{H_2}(cm^{-2})

星形成コア

➔ 大きさや形状に大きな差が見られる

➔ それぞれの原始星に付属する星形成コアが入れ子(d)-(f)

　単純な原始星ー星形成コアペアのみ(a)-(c)

➔ 3次元形状

密度で軸
比上昇

球対称的に膠着

星形成コア内の
構造、密度n>n$_p$
の部分だけを
解析

(a) (c) (f)

0.1pc

γ_{core} (n$_p$>10^5) =1.4 γ_{core}=3.5 γ_{core}=3.3

0.1pc

Star-Forming Cores with Low γ_{core}

フィラメント内
とフィラメント
への膠着

Star-Forming Cores with High γ_{core}

(b) (g) (h)

γ_{core}=15.1 γ_{core}=14.3 γ_{core}=20.4

Count of Star-Forming Cores

120

100

80

60

40

20

n$_p$ > 10^3 cm^{-3}
n$_p$ > 10^4 cm^{-3}
n$_p$ > 10^5 cm^{-3}

1   10   100

Axis Ratio of Star-Forming Cores γ_{core}

軸比

Kohji Tomisaka (NAOJ)
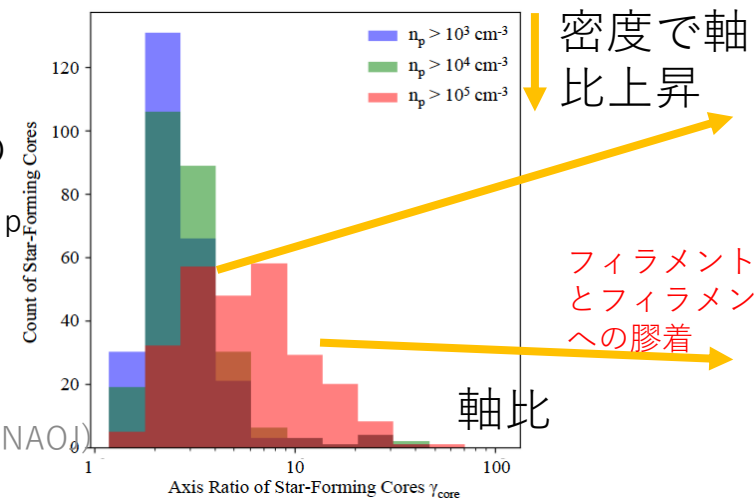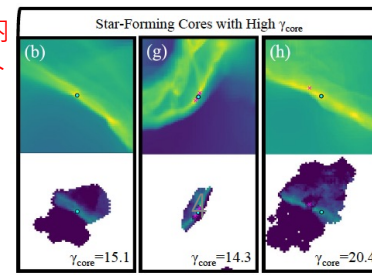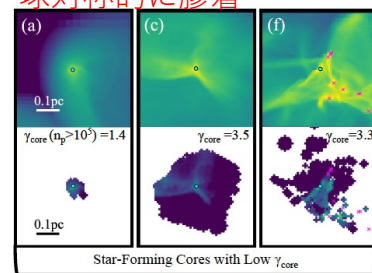
星形成凸多面体内の星形成コアの体積比

$\Phi_{\mathrm{core}} = 11.3\%$ $\Phi_{\mathrm{core}} = 63.3\%$
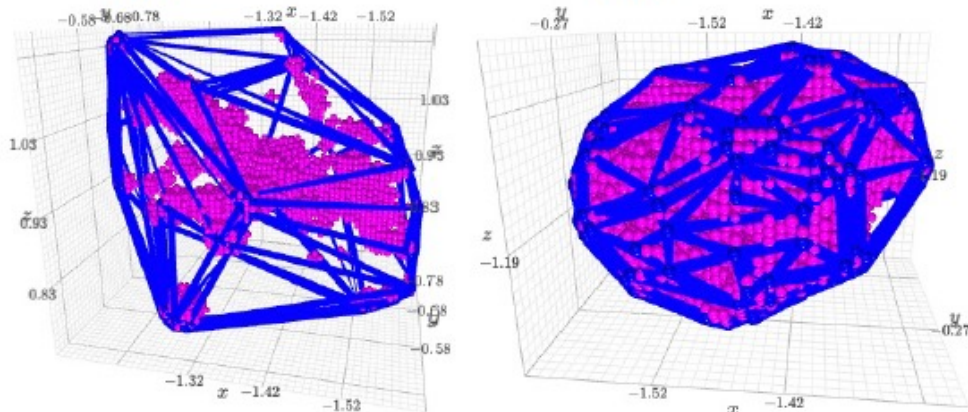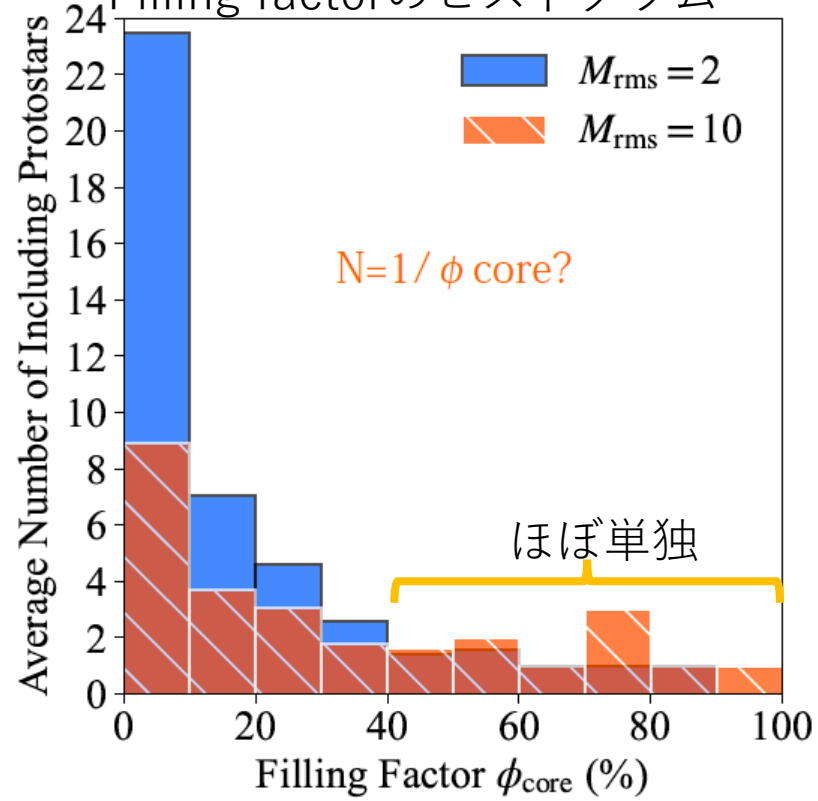
Filling factorと凸多面体の質量の関係
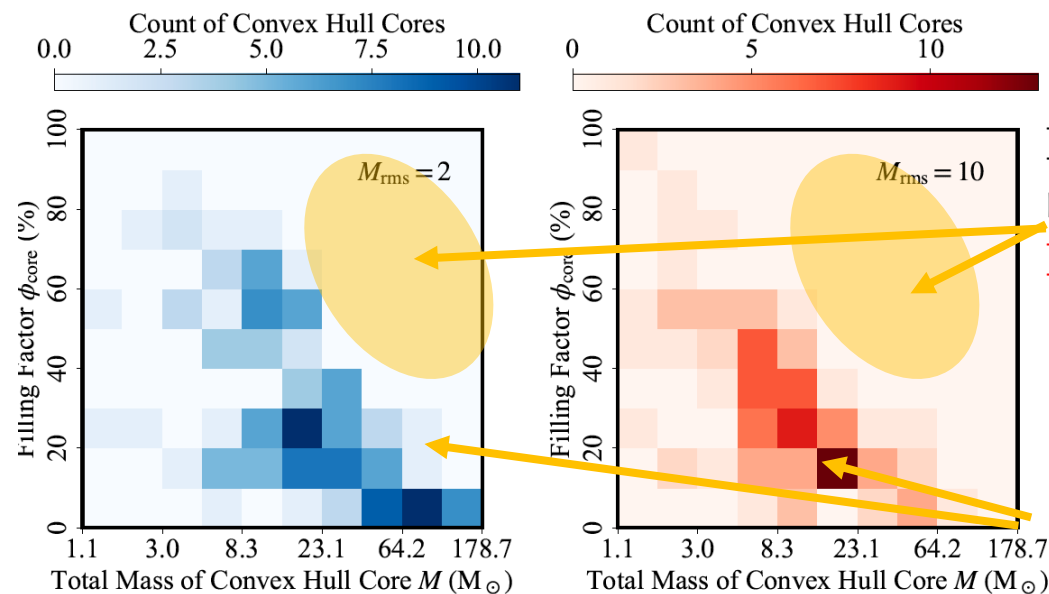
重くて詰まった星形成凸多面体はない

重くて単独原始星を作る星形成凸多面体はない

温度が低すぎ？

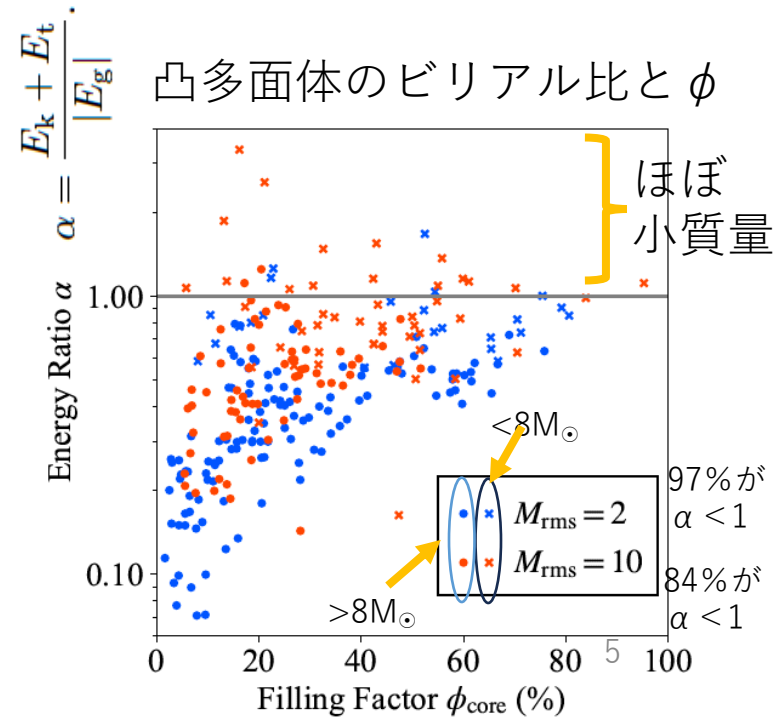重いほど稠密度下がる

Filling factorのヒストグラム

N=1/ φcore?

ほぼ単独

凸多面体のサイズと φ の関係

大きいものは φ が低い
Mに依らない
→乱流の強さに依らない

凸多面体のビリアル比と φ

$\alpha = \dfrac{E_{\mathrm{k}} + E_{\mathrm{t}}}{|E_{\mathrm{g}}|}$

ほぼ小質量

<8M⊙

97%が α<1

>8M⊙

84%が α<1

Kohji Tomisaka (NAOJ)

5

The Fragmentation of Molecular Clouds in Starburst Environments by Matt T. Cusack et al. MNRAS in press

カージフ大
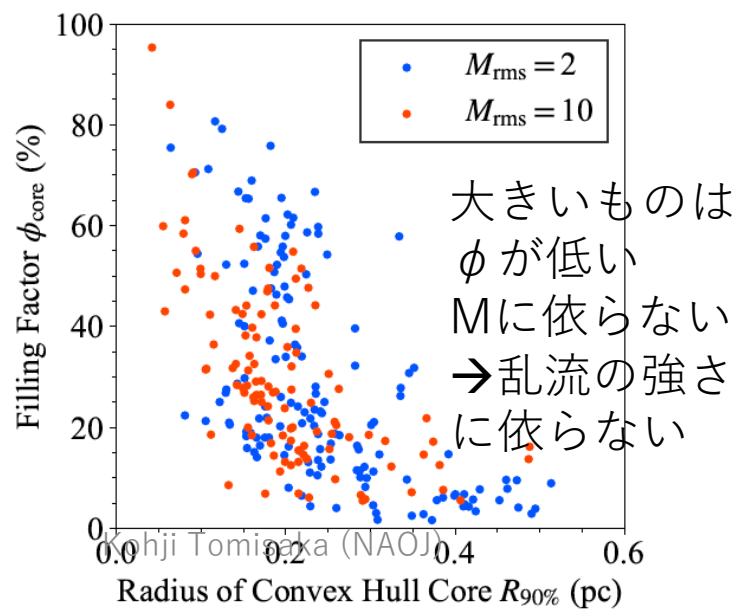
A significant amount of star formation occurs and has occurred in environments unlike the solar neighbourhood. The majority of stars formed closer to the peak of the cosmic star formation rate ($z > 1.3$) and a great deal of star formation presently occurs in the central molecular zone (CMZ) of the Galaxy. These environments are unified by the presence of a high interstellar radiation field (ISRF) and a high cosmic ray ionisation rate (CRIR). Numerical studies of stellar birth typically neglect this fact, and those that do not have thus far been limited in scope. In this work we present the first comprehensive analysis of hydrodynamical simulations of star formation in extreme environments where we have increased the ISRF and CRIR to values typical of the CMZ and starburst galaxies. We note changes in the fragmentation behaviour on both the core and stellar system scale, leading to top-heavy core and stellar system mass functions in high ISRF/CRIR clouds. Clouds fragment less on the core scale, producing fewer but more massive cores. Conversely, the cores fragment more intensely and produce richer clusters of stellar systems. We present a picture where high ISRF/CRIR clouds fragment less on the scale of cores and clumps, but more on the scale of stellar systems. The change in fragmentation behaviour subsequently changes the mass function of the stellar systems that form through enhanced accretion rates.

星間輻射場(ISRF)と
宇宙線電離度(CRIR)が高い
環境での星形成

コアスケール
　分裂しにくくなる
　大きいコアが少数分裂

星スケール
　分裂しやすくなる
　密度の濃い星団を生じる

質量関数をtop-heavyにする

z>1.3の星形成中の銀河
我々の銀河Central Molecular Zone
ULIRGs

星間輻射場、宇宙線電離度の高い環境
での星形成
100〜1000倍

IRSF,CRIRを太陽近傍の1，10，10^2，10^3として乱流を持った雲の進化

γ_1、　γ_{10}、　γ_{100}、　γ_{1000}と名付ける

Simulation	M_0 [M$_\odot$]	R_c [pc]	G [G$_0$]	ξ_{H_2} [s^{-1}]	x_{H_2}
γ_1	1×10^4	4.10	1.7	3.5×10^{-16}	0.358
γ_{10}	1×10^4	4.10	17	3.5×10^{-15}	0.382
γ_{100}	1×10^4	4.10	170	3.5×10^{-14}	0.254
γ_{1000}	1×10^4	4.10	1,700	3.5×10^{-13}	0.046

Kohji Tomisaka (NAOJ)

流体力学＝AREPO (Springel 2010)

シンク粒子　ρ>2x10⁻¹⁶gcm⁻³ r_acc<180au

化学、冷却、加熱　SGCHEM
　輻射輸送効果、各点ごとの外からのΣ、

初期状態　R=4.1pc、M=10⁴M_☉、
　雲　ρ=10³cm⁻³、T_g=40K、T_d=15K
　外部ρ=10cm⁻³、T g=80K

乱流　P(k)∝k-4、E_K=(1/2)E_G

図1　（最初の）シンクセル形成時のΣ分布

複雑な構造

大きな濃いクランプ
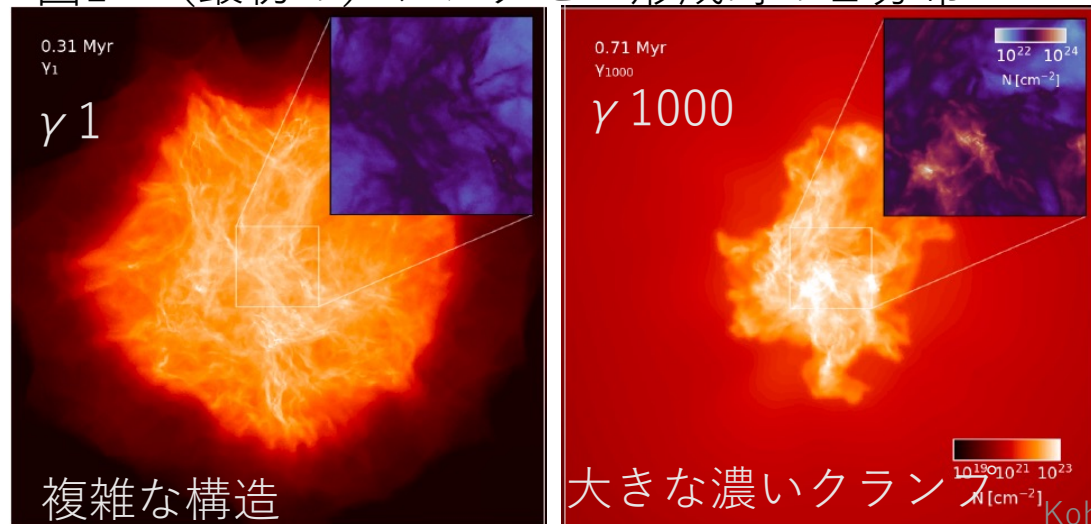
図4シンク粒子質量関数（SMF）
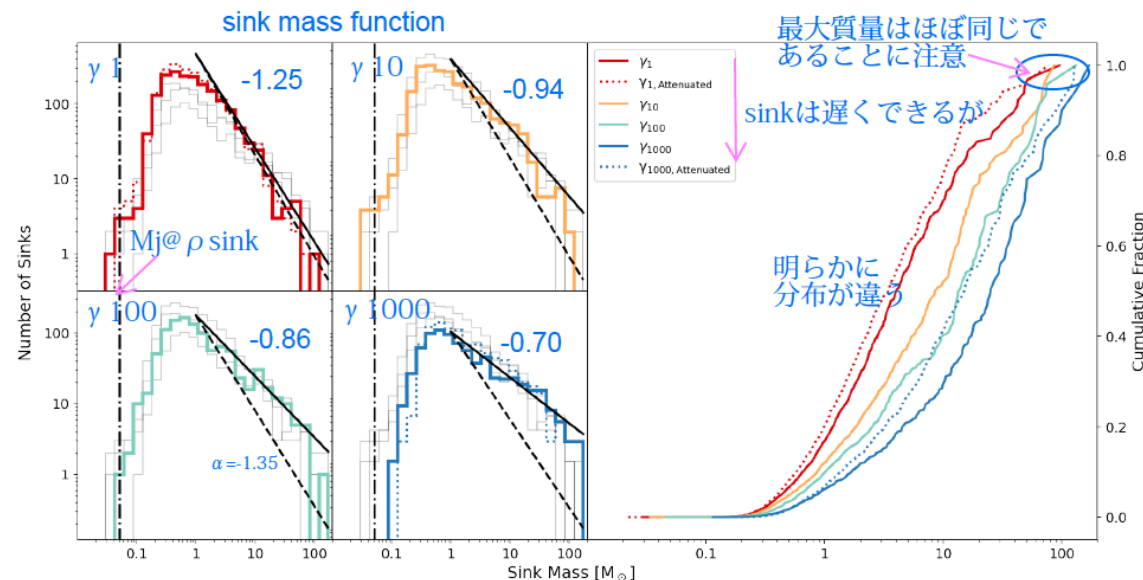
シンク半径が大きいので星の質量関数でないことに注意！円盤分裂過程などの効果が未定
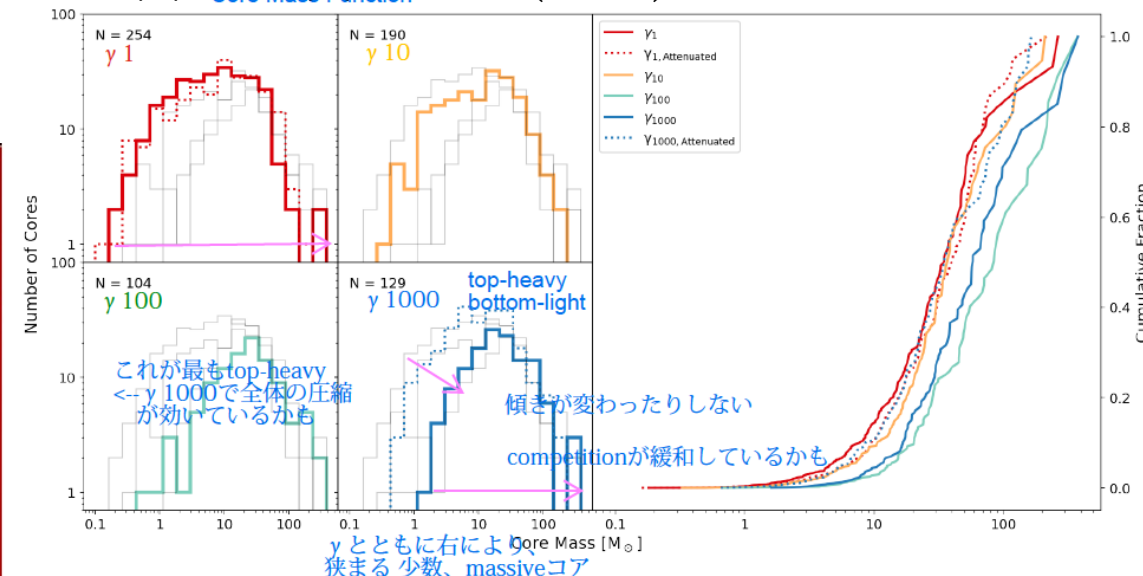
最大質量はほぼ同じであることに注意
sinkは遅くできるが
明らかに分布が違う
Mj@ρ sink
α=-1.35

図8コア質量関数（CMF）

Σ図にdendrogramを掛けた。

これが最もtop-heavy
<-- γ1000で全体の圧縮が効いているかも
top-heavy bottom-light
傾きが変わったりしない
competitionが緩和しているかも
γとともに右により狭まる 少数、massiveコア

Kohji Tomisaka (NAOJ)

7

図3　冷却、加熱率

最終状態のρ-T関係

図2　WNM

図D1　abundance

γ1

等温になる密度は高くなる
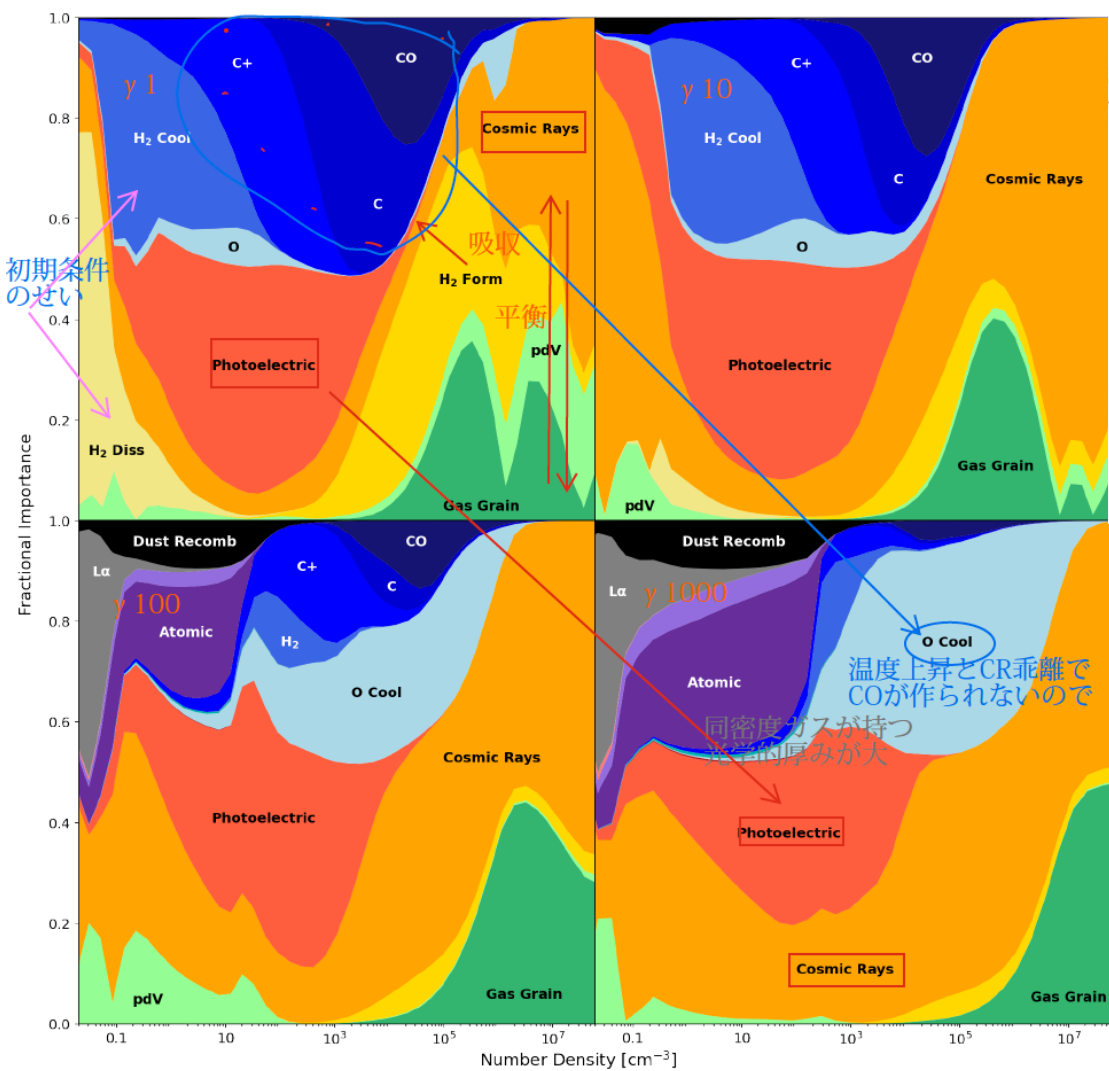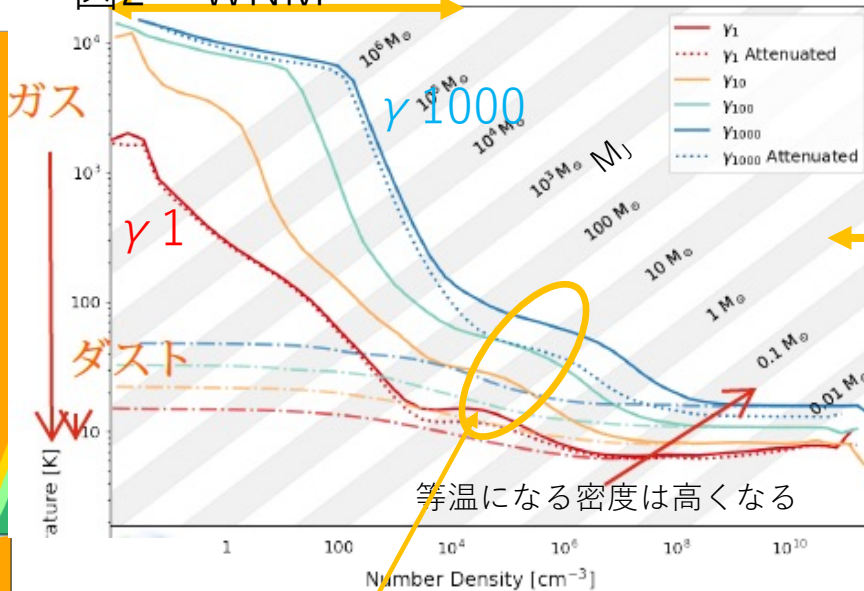
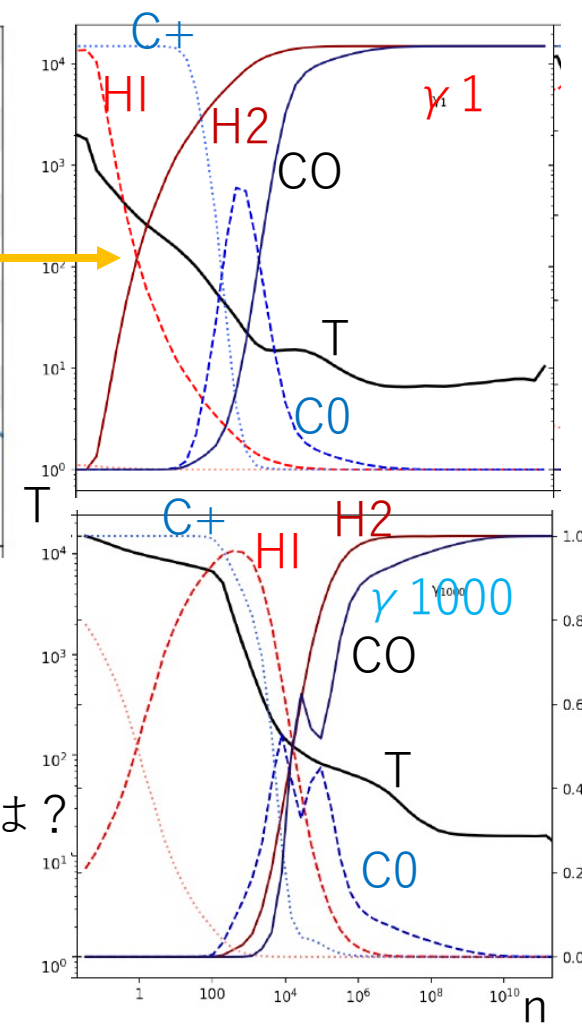M_J
　CMF（図8）は10$M_\odot$位がピーク
　等温「的」な
　このあたりで分裂しているのでは？
　→コア形成
M数
　γ1：等温的部分の温度低、
　　　　マッハ数大、
　　　　小さい構造多数、
　　　　CMF左へ
　γ1000：T高、
　　　　マッハ数小、CMF右へ
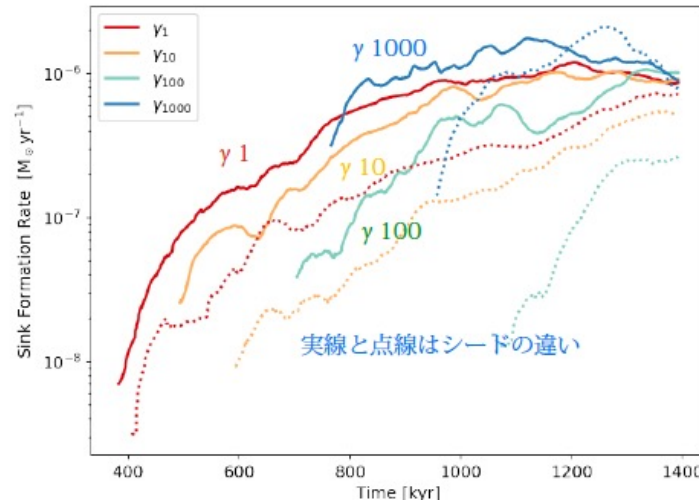
γ1000
H2存在には10^{5}cm^{-5} が
必要
COダークH$_2$ガスはなし

暖色：加熱
寒色：冷却
緑：場合による

温度進化は
λJとM数に影響を与える

初期条件
のせい

温度上昇とCR乖離で
COが作られないので
同密度ガスが持つ
光学的厚みが大

図5 シンク質量と降着率（全シンク、全進化に渡る平均）

Salpeter IMFには dm/dt∝mが必要

dm/dt∝m によく沿う

5個のシンクの進化

dm/dt∝m

dm/dt大

dm/dt∝mよりフラット
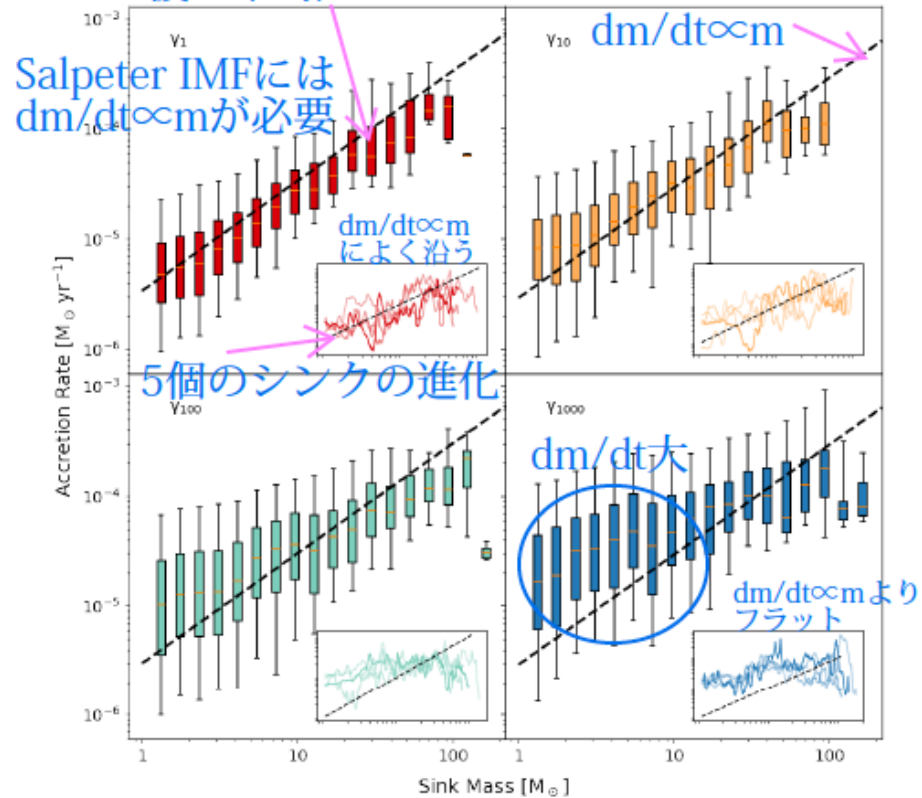
参照 Clark and Whitworth (2021)

図6 シンク形成率＝新規形成率＋降着率

γ_1
γ_{10}
γ_{100}
γ_{1000}

γ 1000
γ 1
γ 10
γ 100

実線と点線はシードの違い

図7

γ 1   γ 10   γ 100   γ 1000

シンク形成時の隣接粒子までの距離

近くなる

10th

5th

1st

5個に分裂

10個に分裂

γとともに多数に分裂

大きなgas reservoirを持つ

競争が激しいので多く残るが、M が小さいわけではない

代表的コアを考える

$n\sim10^5 cm^{-3}$、$T\sim15K$
$\lambda_J\sim10^4 AU$

図7から10^4AUスケールでは
γ1なら5個くらいに
γ1000なら10～10以上に
　分裂しているらしい

・γ1000のコアは温度のせいでもっと大きいだろう
・そのコアはより多くのシンクを含んでいるだろう
・よりリッチな星団を形成するだろう

・コアが同じ質量なら、降着競争の激化によってシンクの質量は少なくなるだろうが
・実際はmassiveなシンクが増える
・これはγ1000のコアにはガスがよりたくさん含むからだろう
　⇔CMFが右に寄っていることに対応

Kohji Tomisaka (NAOJ)

9

$$\frac{\partial N}{\partial m} = A(t)m^{-\alpha}$$

$$\frac{dm}{dt} = Bm^{\beta}$$

$N(>m)$

$\Delta N(t + \Delta t)$

ΔN

m

$m(t)$

$m(t) + \Delta m(t)$

$m(t + \Delta t)$

$m(t + \Delta t) + \Delta m(t + \Delta t)$
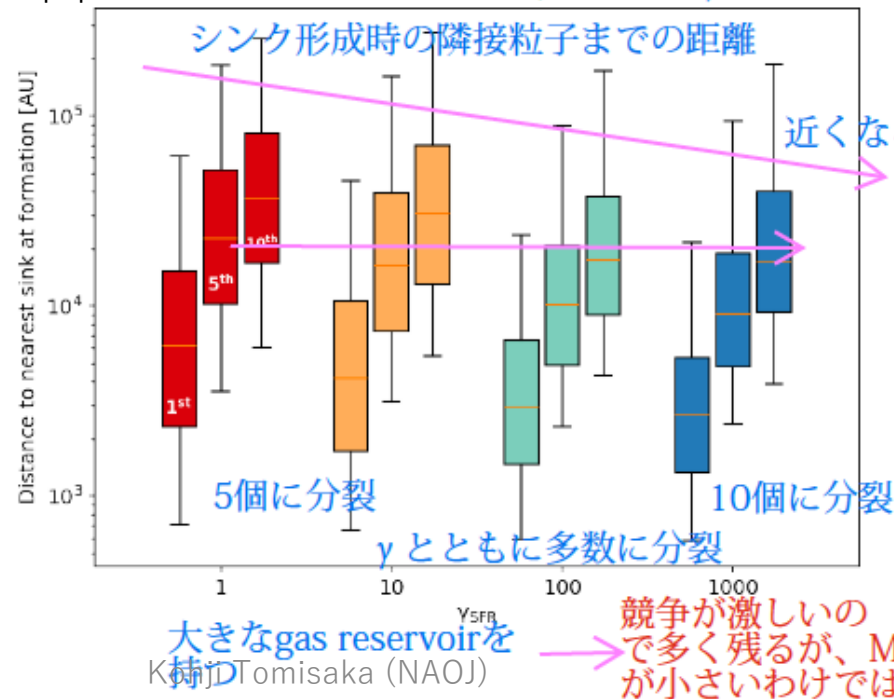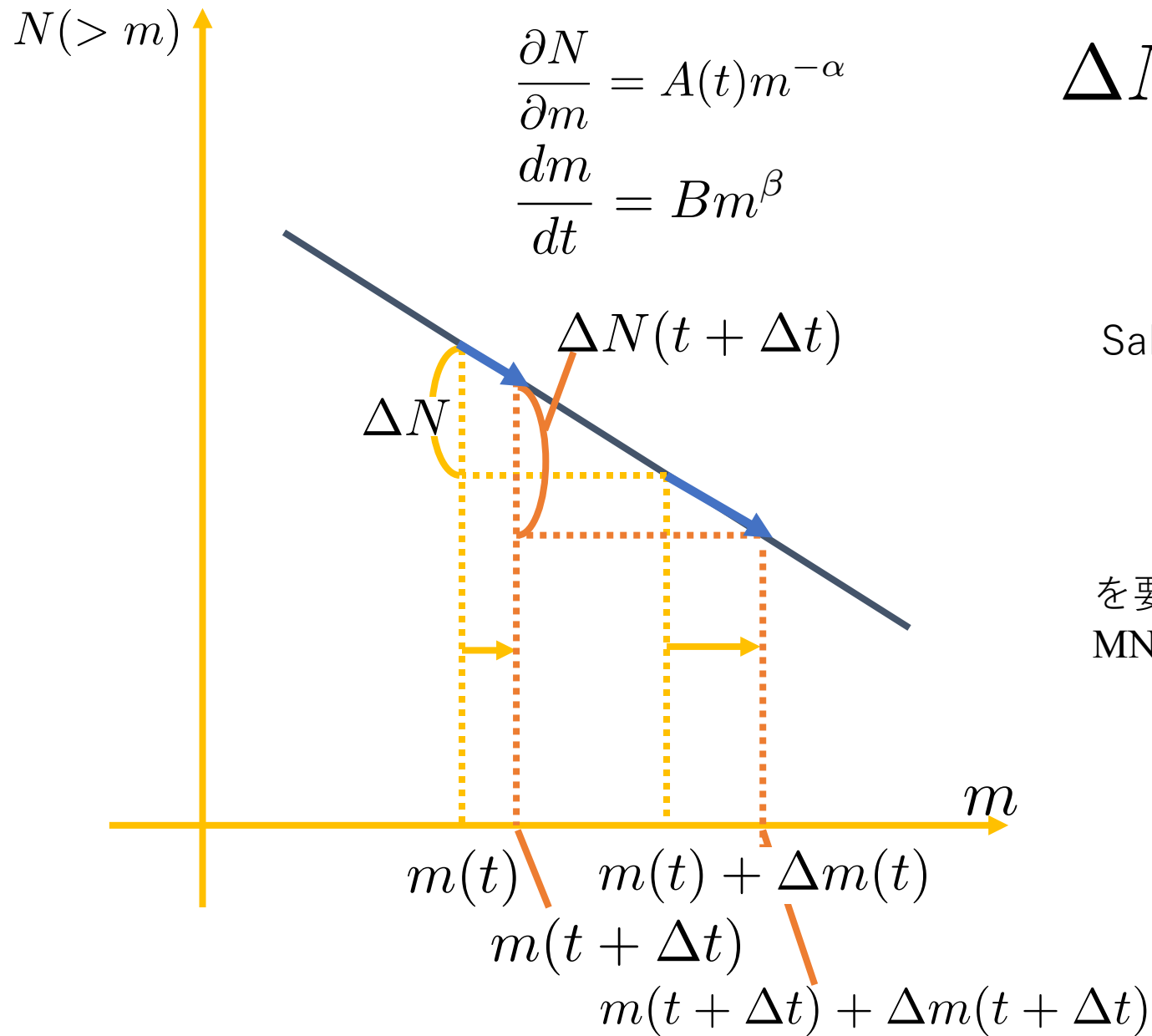
$$\Delta N(t + \Delta t) = \Delta N(t)$$

となるためには、$\beta = 1$が必要

Salpeter(指数関数)型の質量関数は、

$$\frac{dm}{dt} = Bm$$

を要求する（Appendix of Clark and Whitworth; MNRAS 500, 1697–1707 (2021)

GAEP0117-23-50
ALMA chemical survey of disk-outflow sources in Taurus (ALMA-DOT) VII: the layered molecular outflow from HL Tau and its relationship with the ringed disk by F. Bacciotti et al. A & Ap in press
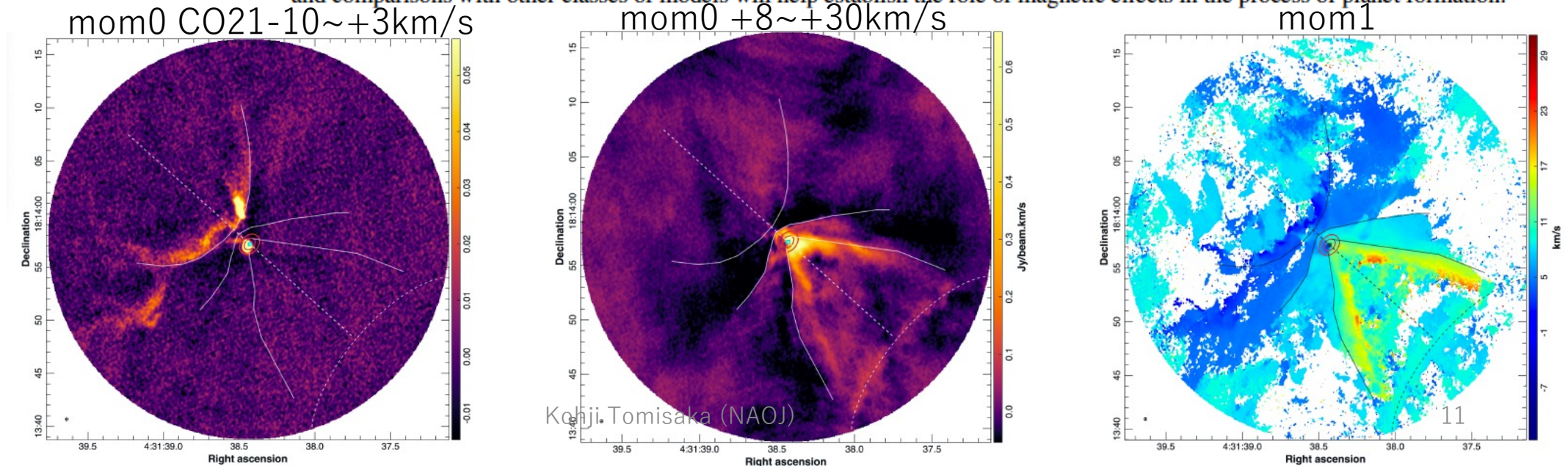
Context. The ALMA image of the ringed disk around HL Tau stands out as the iconic signature of planet formation, but the origin of the observed substructures is still debated. The HL Tau system also drives a powerful bipolar wind, detected in atomic and molecular lines, that may have important feedback on the process.
Aims. The outermost component of the wind traced by CO emission is analyzed in detail to determine its relationship with the disk and its substructures.
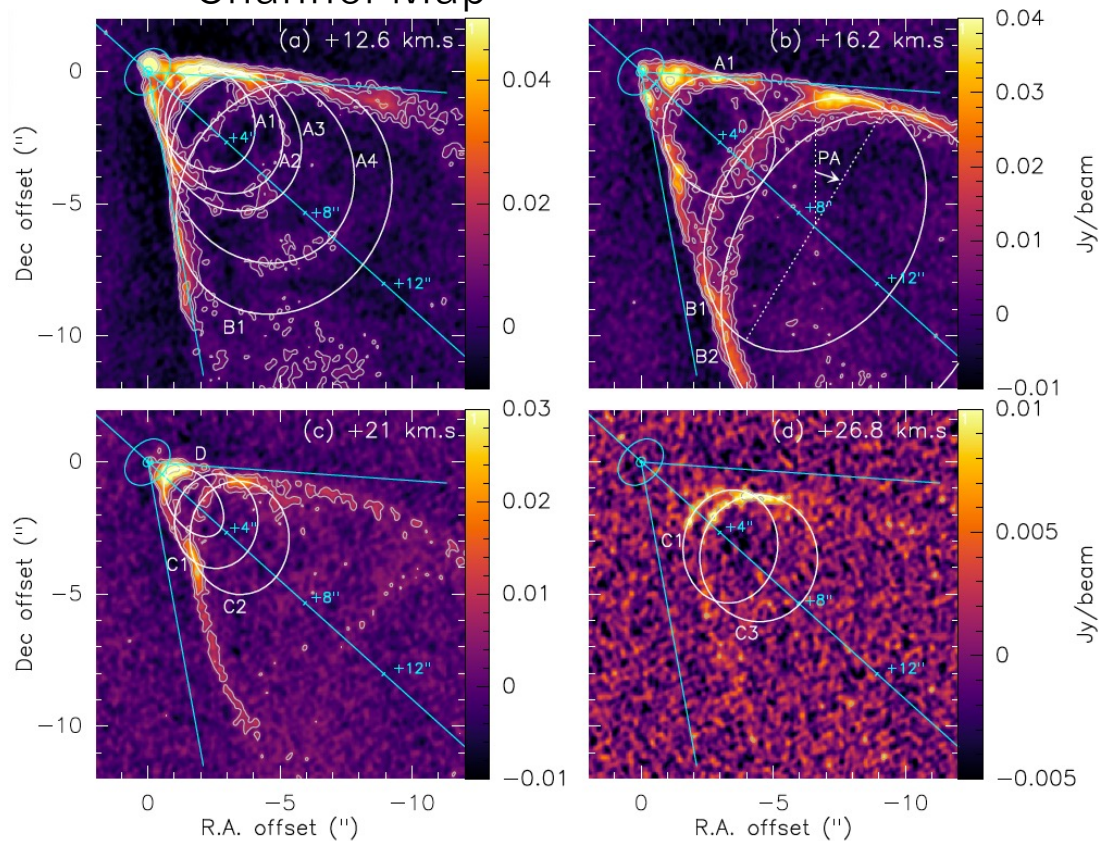*Methods.* A spectro-imaging investigation is conducted using ALMA observations of the ^{12}CO (2-1) line at 1.3 mm, with 0.2 km s^{-1} and $\sim$ 0″28 spectral and angular resolution, in the framework of the ALMA-DOT project. Relevant wind parameters are derived, allowing a tomographic reconstruction of the morphology and kinematics of the red-shifted lobe of the outflow, to compare with theoretical models.
Results. The data channel maps and position-velocity diagrams show a rich substructure of concatenated bubble- and arc-shaped features, whose size and distance from the source continuously increase with velocity. The superposition of such features generates the apparent conical shape. The spatio-kinematical properties suggest that the flow presents distinct nested shells with increasing velocity and faster acceleration going toward the axis, and rotating in the same sense of the disk. The wind parameters are compared with the predictions of magnetohydrodynamic (MHD) disk winds. Under this hypothesis, the launch radii of the three outermost shells are found to be at 55, 67 and 86 au from the star, coincident with regions of enhanced gas density in the disk. We derive a magnetic lever arm $\lambda \sim 4 - 5$, higher than that commonly adopted in models of MHD winds from the outer disk. Interpretations are discussed.
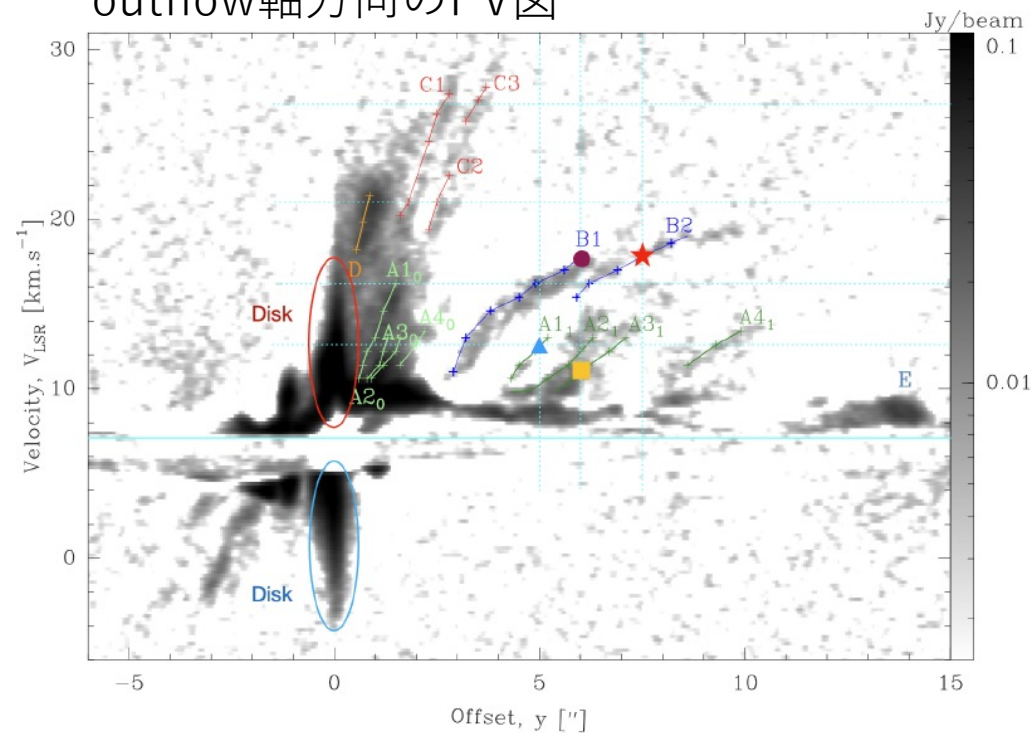*Conclusions.* The properties of the CO outflow from HL Tau appear to be compatible with magnetized disk winds with launch radii in the region at $50 - 90$ au from the source. As such, the wind may be capable of removing angular momentum also from the outer disk. The arrangement of the wind in nested shells with brighter emission rooted in rings of enhanced gas density could support the results of recent non-ideal MHD simulations according to which magnetic instabilities can spontaneously generate both the ring-gap system and a connected inhomogeneous layered wind, alternatively to the action of yet undetected protoplanets. Further observational analyses and comparisons with other classes of models will help establish the role of magnetic effects in the process of planet formation.
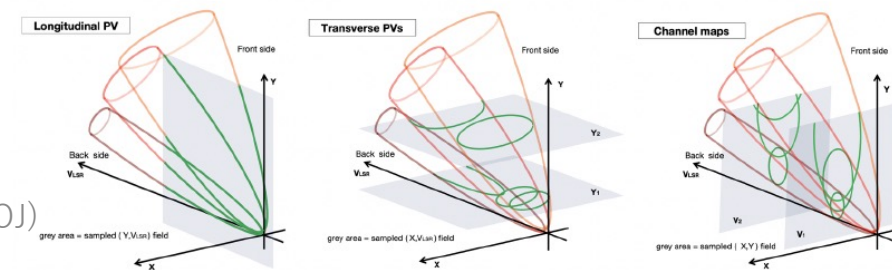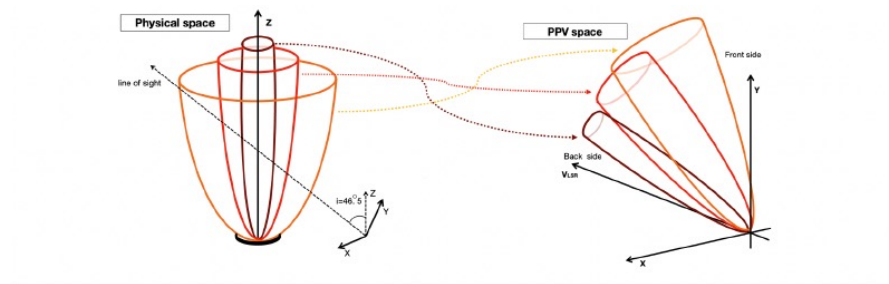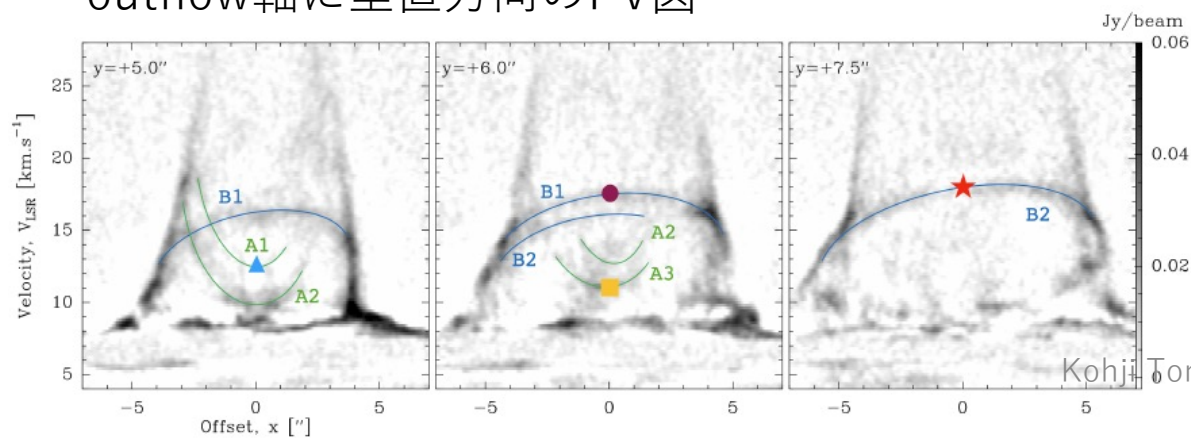
mom0 CO21-10~+3km/s   mom0 +8~+30km/s   mom1

Kohji Tomisaka (NAOJ)

11

Channel Map

outflow軸方向のPV図

outflow軸に垂直方向のPV図

Kohji Tomisaka (NAOJ)

Vertical structure and kinematics of the LMC disc from SDSS/Gaia by O. Jimenez-Arranz et al. AAp in press

Context. Studies of the LMC's internal kinematics have provided a detailed view of its structure, largely thanks to the exquisite proper motion data supplied by the *Gaia* mission. However, line-of-sight (LoS) velocities, the third component of the stellar motion, are only available for a small subset of the current *Gaia* data, limiting studies of the kinematics perpendicular to the LMC disc plane.
Aims. We synergise new *SDSS*-IV/V LoS velocity measurements with existing *Gaia* DR3 data, increasing the 5D phase-space sample by almost a factor of three. Using this unprecedented dataset, we interpret and model the vertical structure and kinematics across the LMC disc.
Methods. We first split our parent sample into different stellar types (young and old). We then examine maps of vertical velocity, $v_{z'}$, moments (median and MAD) perpendicular to the LMC disc out to $R' \approx 5$ kpc; we also examine the vertical velocity profiles as a function of disc azimuth and radius. We interpret our results in the context of three possible scenarios: 1) time-variability in the orientation of the disc symmetry axis; 2) use of an incorrect LMC disc plane orientation; or 3) the presence of warps or twists in the LMC disc. We also present a new inversion method to construct a continuous 3D representation of the disc from spatially-resolved measurements of its viewing angles.
*Results.* Using young stellar populations, we identify a region in the LMC arm with highly negative $\overline{v_{z'}}$; this overlaps spatially with the supershell LMC 4. When interpreting the maps of $\overline{v_{z'}}$, our results indicate that: 1) the LMC viewing angles may vary with time due to, e.g., precession or nutation of the spin axis, but this cannot explain most of the structure in $\overline{v_{z'}}$ maps; 2) when re-deriving the LMC disc plane by minimising the RMS vertical velocity $v_{z'}$ across the disc, the inclination and line-of-nodes position angle are $i = 24°$ and $\Omega = 327°$, respectively, with an $\sim 3°$ systematic uncertainty associated with sample selection, contamination, and the position of the LMC center; 3) when modelling in concentric rings, we obtain different inclinations for the inner and outer disc regions, and when modelling in polar segments we obtain a quadrupolar variation as function of azimuth in outer the disc. We provide 3D representations of the implied LMC disc shape. These provide further evidence for perturbations caused by interaction with the SMC.
Conclusions. The combination of *SDSS*-IV/V and *Gaia* data reveal that the LMC disc is not a flat plane in equilibrium, but that the central bar region is tilted relative to a warped outer disc.
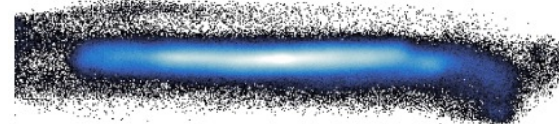
Gaia DR3＋SDSS
赤方偏移データ

LMCのディスクの
星のz方向速度分布を
調べた。

warped disk
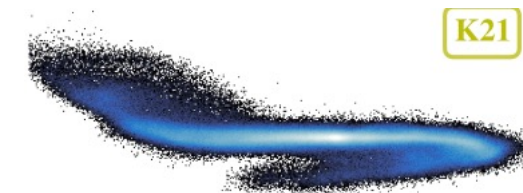
tilted bar

JOYS: The [D/H] abundance derived from protostellar outflows across the Galactic disk measured with JWST by L. Francis et al, A&Ap in press

Context. The total deuterium abundance [D/H] in the universe is set by just two processes: the creation of deuterium in Big Bang Nucleosynthesis at an abundance of [D/H]= $2.58 \pm 0.13 \times 10^{-5}$, and its destruction within stellar interiors (astration). Measurements of variations in the total [D/H] abundance can thus potentially provide a probe of Galactic chemical evolution. However, most observational measurements of [D/H] are only sensitive to the gas-phase deuterium, and the amount of deuterium sequestered in dust grains is debated. With the launch of the James Webb Space Telescope (JWST), it is now possible to measure the gas-phase [D/H] at unprecedented sensitivity and distances through observation of mid-IR lines of H_2 and HD. Comparisons of gas-phase [D/H] with the constraints on the total [D/H] from the primordial abundance and Galactic chemical evolution models can provide insight into the degree of Deuterium lock-up in grains and the star formation history of our Galaxy.

Aims. We use data from the JWST Observations of Young protoStars (JOYS) program of 5 nearby and resolved low-mass protostellar outflows and 5 distant high-mass protostellar outflows taken with the JWST Mid Infrafred Instrument (MIRI) Medium Resolution Spectrometer (MRS) to measure gas-phase [D/H] via H_2 and HD lines, assuming the gas is fully molecular.

Methods. We extract spectra from various locations in the outflows. Using a rotational diagram analysis covering lines of H_2 and HD with similar excitation energies, we derive the column density of HD and H_2 or their upper limits. We then calculate the gas-phase [D/H] from the column density results, and additionally apply a correction factor for the effect of chemical conversion of HD to atomic D and non-LTE excitation on the HD abundance in the shocks. To investigate the spatial distribution of the bulk gas and species refractory species associated with the dust grains, we also construct integrated line intensity maps of H_2, HD, [Fe II], [Fe I], and [S I] lines.

Results. A comparison of gas-phase [D/H] between our low-mass sources shows variations of up to a factor of ~ 4, despite these sources likely having formed in nearly the same region of the Galactic disk that would be expected to have nearly constant total [D/H]. Most measurements of gas-phase [D/H] from our work or previous studies produce [D/H] $\lesssim 1.0 \times 10^{-5}$, a factor of $2-4$ lower than found from local UV absorption lines and as expected from Galactic chemical evolution models. In the integrated line intensity maps, the morphology of the HD R(6) line emission is strongly correlated with the H_2 S(7), [S I], and [Fe I] lines which mostly trace high velocity jet knots and bright bow-shocks. In our extracted spectra along the outflows, there is similarly a strong correlation between the H_2 and HD column density and the [S I] and [Fe I] line flux, however, no correlation is seen between [D/H] and the [S I] or [Fe I] line flux.

Conclusions. The variations in [D/H] between our low-mass sources and the low [D/H] with respect to Galactic chemical evolution models suggest that our observations are not sensitive to the total [D/H]. Significant depletion of deuterium onto carbonaceous dust grains is a possible explanation, and tentative evidence of enhanced [D/H] towards positions with higher gas-phase Fe abundance is seen in the HH 211 outflow. Deeper observations of HD and H_2 across a wider range of shock conditions and modelling of the carbonaceous dust-grain destruction and shock conditions are warranted to test for the effects of depletion.

protostellar outflowの中間赤外
HD, H2回転遷移線
JWST観測
我々の銀河の現在の[D/H]に関する情報

D原子は炭素質ダスト表面にH原子より吸着しやすい」という効果を見ている。

14

Detectability of Emission from Exoplanet Outflows Calculated by pyTPCI, a New 1D Radiation-Hydrodynamic Code by Riley Rosener et al. ApJ in press

Photoevaporation in exoplanet atmospheres is thought to contribute to the shaping of the small planet radius valley. Escaping atmospheres have been detected in transmission across a variety of exoplanet types, from hot Jupiters to mini-Neptunes. However, no work has yet considered whether outflows might also be detectable in emission. We introduce pyTPCI, a new, open-source self-consistent 1D radiative-hydrodynamics code that is an improved version of The PLUTO-CLOUDY Interface. We use pyTPCI to model seven exoplanets (HD 189733b, HD 209458b, WASP-69b, WASP-107b, TOI-1430b, TOI-560b, and HAT-P-32b) at varying metallicities and compute their emission spectra to investigate their detectability across a variety of spectral lines. We calculate the eclipse depths and signal-to-noise ratios (SNR) of these lines for a 10m class telescope with a high-resolution spectrograph, taking into account appropriate line broadening mechanisms. We show that the most detectable spectral lines tend to be the 589 nm Na I doublet and the 1083 nm metastable helium triplet. Hα and Mg I 457 nm are moderately strong for some planets at some metallicities, but they are almost always optically thin, so some of their emission may not be from the outflow. The planet with the highest-flux, highest-eclipse-depth, and highest-SNR lines is HD 189733b, with a Na I eclipse depth of 410 ppm and SNR of 2.4 per eclipse, and a He* eclipse depth of 170 ppm and SNR of 1.3. These signals would be marginally detectable with Keck if 3–10 eclipses were observed, assuming (over-optimistically) photon limited observations.

中心星を起源とする系外惑星大気の光蒸発

トランジット時の吸収スペクトルでなく、輝線で見えるかを計算した。